Bio-resin for High Resolution Lithography-based Biofabrication of Complex Cell Laden Constructs

Khoon S. Lim[+], Riccardo Levato[+], Pedro F. Costa, Miguel D. Castilho, Cesar R. Alcala-Orozco, Kim M. A. van Dorenmalen, Ferry P.W. Melchels, Debby Gawlitta, Gary J. Hooper, Jos Malda, Tim B. F. Woodfield[*]*

Dr. K. S. Lim, C. R. Alcala-Orozco, Prof. G. J. Hooper, Prof. Dr. T. B. F. Woodfield

Christchurch Regenerative Medicine and Tissue Engineering (CReaTE) Group, Department of Orthopaedic Surgery and Musculoskeletal Medicine, University of Otago Christchurch, Christchurch 8011, New Zealand

E-mail: khoon.lim@otago.ac.nz, tim.woodfield@otago.ac.nz

Dr. R. Levato, Dr. P. F. Costa, Dr. M. D. Castilho, K. V. Dorenmalen, Prof. J. Malda

Department of Orthopaedics, University Medical Center Utrecht, The Netherlands

Dr. D. Gawlitta

Department of Oral and Maxillofacial Surgery and Special Dental Care, University Medical Center Utrecht, The Netherlands

Dr. F. P. W. Melchels

Institute of Biological Chemistry, Biophysics and Bioengineering, Heriot-Watt University, Edinburgh, United Kingdom

[+]Equal author contribution: K. S. Lim, R. Levato

Abstract

Lithography-based three-dimensional (3D) printing technologies allow high spatial resolution that exceeds that of typical extrusion-based bioprinting approaches, allowing to better mimic the complex architecture of biological tissues. Additionally, lithographic printing via digital light processing (DLP) enables fabrication of free-form lattice and patterned structures which cannot be easily produced with other 3D printing approaches. While significant progress has been dedicated to the development of cell-laden bioinks for extrusion-based bioprinting, less attention has been directed towards the development of cyto-compatible bioresins and their application in lithography-based biofabrication, limiting the advancement of this promising technology. In this study, we developed a new bioresin based on methacrylated poly(vinyl alcohol) (PVA-MA), gelatin methacryloyl (Gel-MA) and a transition metal-based visible light photo-initiator. The utilization of a visible light photo-initiating system displaying high molar absorptivity allowed the bioprinting of constructs with complex, high resolution features, in the range of 25-50μm. Biofunctionalization of the resin with Gel-MA allowed long term survival of encapsulated cells, and enabled attachment and spreading of endothelial cells seeded on the printed hydrogels. Furthermore, 3D biofabrication of cell-laden hydrogel constructs with ordered architecture was successfully demonstrated, where the encapsulated cells remained viable, homogenously distributed and functional. Osteogenic and chondrogenic tissue formation was confirmed following long-term culture of encapsulated stem cells, underlining the potential of these DLP-bioprinted hydrogels for tissue engineering and biofabrication. Overall, the PVA-MA/Gel-MA bioresin is a promising material for biofabrication and provides important cues for the further development of lithography-based bioprinting of complex, free-form living tissue analogs.

Keywords: biofabrication, lithography, bio-resin, hydrogel, digital light processing

1. Introduction

Over the past decade, three-dimensional (3D) biofabrication demonstrated potential to fabricate cell-laden hydrogel constructs by the hierarchical layer-by-layer assembly of cells and extra-cellular matrix components, with the aim to engineer functional tissues [1,2]. The most commonly reported strategies in biofabrication using cell-laden hydrogels, also termed bioinks, include extrusion-based or jetting-based 3D bioprinting approaches [3–6]. Often, bioinks are co-printed with thermoplastic polymers and/or sacrificial support materials to generate anatomical structures and hybrid, multi-material constructs [7,8]. However, these technologies have limited resolution, dictated by the gauge of the extrusion nozzle, shear stress imposed to the extruded cells, and are characterized by relatively slow printing time. Lithography-based bioprinting technologies, such as stereolithography (SLA) or digital light processing (DLP), represent versatile alternative approaches for shaping photo-sensitive biomaterials into complex 3D constructs. Importantly, these technologies allow high spatial resolution exceeding that of extrusion-based bioprinting approaches, and thereby offering the potential to better mimic the complex architecture and micro-environment of biological tissues [9–12]. However, while significant recent progress has focused on the development of cell-laden bioinks for extrusion-based bioprinting, with an associated improvement in our understanding of bioink rheological properties that define a successful biofabrication window [7,13,14], less attention has been directed towards the development of cyto-compatible, cell-laden bio-resins and their application in lithography-based biofabrication [10,11,15].

Lithography-based fabrication via digital light processing (DLP) adopts a digital micro-mirror device to project a patterned mask of light (usually in the UV or visible range) onto the bottom surface of a polymer resin bath in contact with an inverted build platform, thereby photo-polymerizing specific regions of the resin via light exposure. The platform then moves stepwise in the z-direction (vertically), with subsequent flow of the resin to achieve a fresh resin level before repeating the process [16,17]. The incorporation of an appropriate biocompatible photo-polymerizable hydrogel

precursor solution, photo-initiators and cells into the resin – defined herein as a bio-resin – results in high resolution biofabrication of a 3D cell-laden construct using a layer-by-layer approach. The reported maximum resolution of DLP is within the range of 25 – 50μm [10]. However, the full capacity of lithography-based biofabrication technologies demonstrating the ability to fabricate cyto-compatible, cell-laden hydrogels of defined architecture at these length scales (<50μm) has not yet been realized. Therefore, the aim of this study was to develop a novel biofunctional, photo-polymerizable bio-resin for biofabrication of thick, cell-laden hydrogel constructs with high spatial resolution and defined architectures, even when using commercial DLP printing technology. A photoresponsive methacrylated poly(vinyl alcohol) (PVA-MA), biofunctionalized with gelatin-methacryloyl (gelMA) was used as a platform hydrogel for DLP biofabrication, activated via highly efficient visible light initiators, enabling the generation of accurate hydrogel structures, with superior spatial resolution, that cannot be obtained with other bioprinting techniques.

2. Materials and Methods

2.1 Synthesis of PVA-MA

PVA-MA was prepared by reacting PVA (Sigma-Aldrich, 13-23kDa, 98% hydrolysed) with methacrylic anhydride (Sigma) in water. A 10wt% solution of PVA (50g) in water (500ml) was heated to 80°C until the PVA was completely dissolved. The PVA solution was then left to cool to room temperature prior to the addition of methacrylic anhydride (18.75ml) and the mixture was left to react for 48 hours. The pH of the reaction solution was adjusted to 8. To stop the reaction, the solution was precipitated in toluene. The precipitated polymer was re-dissolved in water and then purified by ultrafiltration through a 10kDa molecular weight cut-off membrane (Sigma). Lastly, the purified solution was sterilised by filtration and lyophilized. The degree of methacrylation of PVA was calculated by comparing the area of the methacrylate vinyl proton peak, $\delta = 6.1$ (s, H^1) and 5.8 (s, H^2) to the area of the protons in the PVA backbone, $\delta = 4.0$ (s, H^3), using 1H-proton nuclear magnetic resonance spectroscopy (Bruker Avance 400 MHz).

2.2 Synthesis of Gel-MA

Gelatine (Sigma-Adrich, porcine skin, 300g bloom strength) was dissolved in PBS at a 10wt% concentration. 0.6g of methacrylic anhydride per gram of gelatine was added to the gelatine solution, and left to react for 1h at 50˚C under constant stirring, followed by dialysis against deionised water to remove unreacted methacrylic anhydride. The purified Gel-MA solution was sterile-filtered and lyophilised. The degree of methacryloyl substitution was quantified to be 60% using 1H-proton nuclear magnetic resonance spectroscopy.

2.3 3D printing using DLP and construction of working curve

Constructs were fabricated using the Perfactory® 3 Mini (EnvisionTec, Gladbeck, Germany). The final bio-resin formulation used was 10wt% PVA-MA + 1wt% photo-absorber (Ponceau 4R) with or without 1wt% Gel-MA. The photoinitiator concentration was 0.2mM/2mM Ru/SPS. (tris-bipyridyl-ruthenium (II) hexahydrate, Ru) combined with a persulfate compound (sodium persulfate, SPS). Solid shapes and complex porous constructs were first designed with a CAD software (Tinkercad, Autodesk, USA) or downloaded as STL files from existing repositories. Constructs were printed by exposing each layer (50μm) to 10 seconds of 7.25mW cm^{-2} of visible light, using a step size of 25-50 μm. A schematic of the DLP bioprinting set-up is reported in Figure 1.

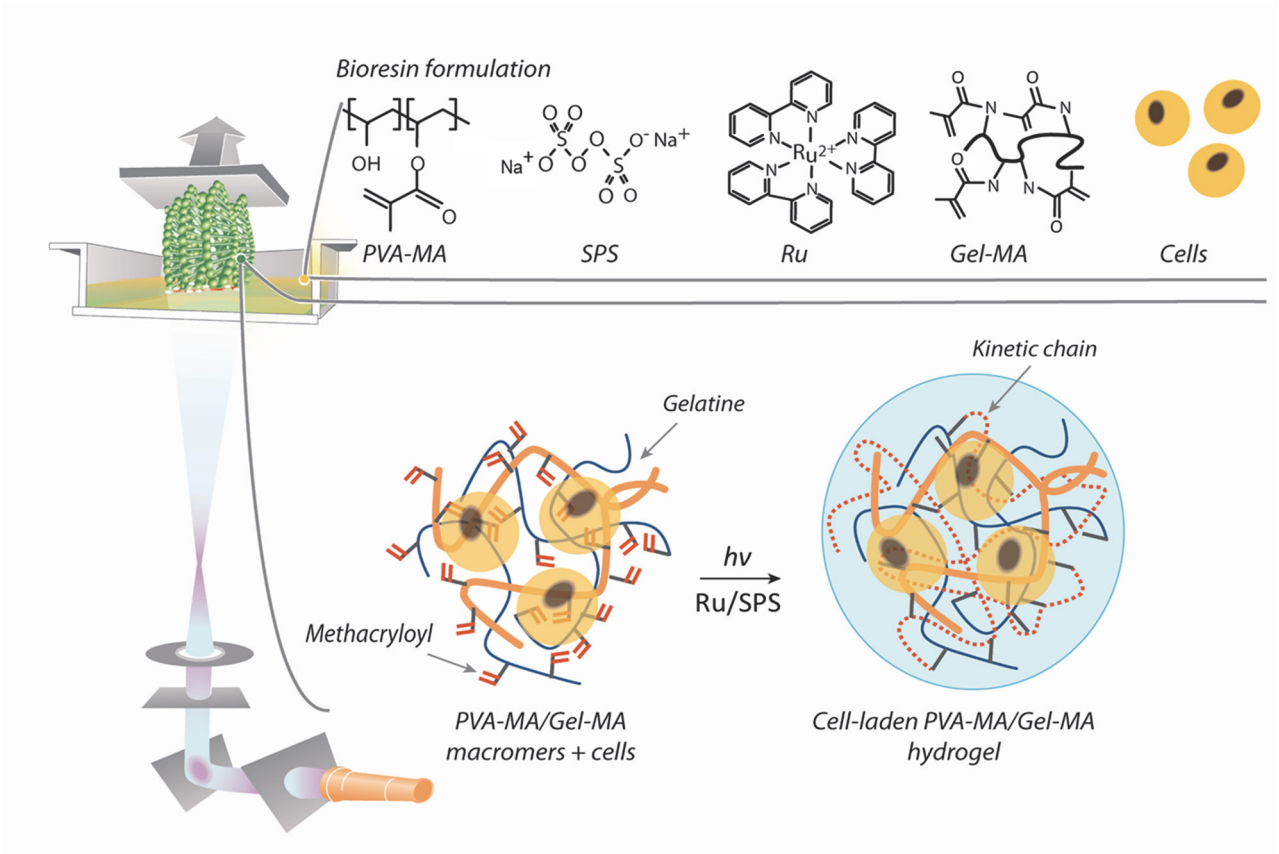

Figure 1. Scheme of top-down biofabrication approach in a DLP apparatus. Inset shows the compounds in the bio-resin : methacrylated poly(vinyl alcohol) (PVA-MA), gelatin-methacryloyl (Gel-MA), tris-bipyridyl ruthenium hexahydrate (Ru) and sodium persulfate (SPS).

The bio-resin formulation used to construct the working curve is 10wt% PVA-MA + 0.2mM/2mM Ru/SPS, with and without the photo-absorber (1wt% Ponceau 4R). The bio-resin was pipetted onto a glass slide and then exposed to a range of irradiation dosages (E = light intensity x exposure time) using the Perfactory 3 Mini (EnvisionTec, Gladbeck, Germany). The thickness of the crosslinked layer (cure depth) was measured. The working curve is defined by the plot of cure depth versus the irradiation dosage and is given by the equation 1, where C_d is the cure depth, D_p is the light penetration depth, and E_c is the critical energy required to reach the gel point.

$$C_d = D_p \, ln\frac{E}{E_c} \qquad \text{(eq 1)}$$

2.4 Sol-gel analysis and physical characterization of the bio-resin and DLP 3D printed hydrogels

Viscosity of the bio-resin, with or without 1wt% Gel-MA, was determined with a DHR2 rheometer (TA Instruments, Etten-Leur, The Netherlands), by subjecting samples of the uncrosslinked resin to a continuous flow at a shear rate of 200 s^{-1} for a duration of 120 s. Next, cylindrical, non-porous samples (5 mm diameter and 1 mm height) with or without Gel-MA, were prepared as described in the previous section, to perform sol-gel analysis, in order to evaluate the physico-chemical and mechanical properties of the printed constructs. Mass loss and swelling studies were conducted according to previously published protocols. Directly after printing, all samples were weighed for the initial wet mass ($m_{\text{initial, t0}}$) and three samples were immediately lyophilised to obtain their dry weights ($m_{\text{dry ,t0}}$). The actual macromer concentration was calculated based on equation 2:

$$\%\, macromer = \frac{m_{dry,t0}}{m_{initial,t0}}\, 100\% \qquad \text{(eq 2)}$$

These samples were then submerged in a excess volume of PBS, incubated, and weighed ($m_{swollen}$) after 1 day. The swollen samples were then freeze-dried and weighed again (m_{dry}). The mass swelling ratio (q) and mass loss were calculated as follows:

$$\%\, mass\ loss = \frac{m_{i,dry} - m_{dry}}{m_{i,dry}}\, 100\% \qquad \text{(eq 3)}$$

$$q = \frac{m_{swollen}}{m_{dry}} \qquad \text{(eq 4)}$$

The sol fraction which is a measurement of the macromers not crosslinked into the hydrogel network is given by the mass loss at 1 day [18]. The crosslinking density (ρ_x) was calculated using a modified Flory-Rehner equation as follows [19]:

$$\frac{1}{\overline{M_c}} = \frac{2}{\overline{M_n}} - \frac{\left(\frac{\bar{v}}{V_1}\right)\left[\ln\left(1 - v_{2,s}\right) + v_{2,s} + \chi v_{2,s}^2\right]}{v_{2,r}\left[\left(\frac{v_{2,s}}{v_{2,r}}\right)^{\frac{1}{3}} - \frac{1}{2}\left(\frac{v_{2,s}}{v_{2,r}}\right)\right]} \qquad \text{(eq 5)}$$

$$(\bar{r}_0^2)^{\frac{1}{2}} = l\left(\frac{2\overline{M_c}}{M_r}\right)^{\frac{1}{2}} C_n^{\frac{1}{2}} \qquad \text{(eq 6)}$$

$$\xi = \upsilon_{2,s}^{-\frac{1}{3}} \ (\bar{r}_0^2)^{\frac{1}{2}} \quad \text{(eq 7)}$$

$$\rho_x = \frac{1}{\bar{\upsilon}\overline{M_c}} \quad \text{(eq 8)}$$

Where $\overline{Mc}$: number average molecular weight between crosslinks, $\overline{Mn}$: number average molecular weight in the absence of any crosslinking (16000 g mol^{-1} for PVA), $\bar{\upsilon}$: specific volume of the polymer (0.788 m^3 kg^{-1} for PVA), V_1: molar volume of the solvent, $\upsilon_{2,s}$: equilibrium polymer volume fraction, $\upsilon_{2,r}$: polymer volume fraction after crosslinking, $(\bar{r}_0^2)^{1/2}$: end to end distance of the unperturbed (solvent free) state of the polymer, χ: polymer solvent interaction (0.49 for PVA in water), l: bond length (1.54Å for PVA c-c bond), M_r: molecular weight of the repeating unit (44 for PVA), C_n: characteristic ratio (8.9 for PVA).

Mechanical properties of the printed gels were evaluated with a Dynamical Mechanical Analyser (DMA, Q800, TA Instruments) in a uni-axial, unconfined compression test. Briefly, the cylindrical samples were compressed up to 30% deformation at a strain rate of 20%/minute. Compression modulus was defined as the slope of the stress strain curve in the linear range between 10 and 15% strain.

DLP 3D printed scaffolds were sputter coated with carbon (Electron Microscopy Sciences, EMS150T), following scanning electron microscopy (SEM) imaging using a Jeol JSM 7000F FE-SEM with secondary electron detection used at an acceleration voltage of 15kV.

2.5. Cell isolation and culture

Human endothelial colony-forming progenitor cells (ECFCs) were derived from human umbilical cord blood (following a previously published protocol) [20], while human mesenchymal stromal cells (MSCs) were obtained from bone marrow aspirates and characterized as previously reported [21]. Patient material was received upon informed consent and obtained in agreement with patient data protection and ethical guidelines of the local Medical Ethics Committee (University Medical Center Utrecht). ECFCs were cultured on collagen-coated plates in Endothelial Growth

Medium (EGM), containing EGM-2 (Lonza, Breda, the Netherlands) supplemented with 10% heat-inactivated fetal calf serum (FCS, Lonza), 100U ml^{-1} penicillin, 100µg ml^{-1} streptomycin (Life Technologies), and Single Quots (EGM-2 BulletKit (CC-3162) containing hEGF, Hydrocortisone, GA-1000 (Gentamicin, Amphotericin-B), VEGF, hFGF-B, R3-IGF-1, Ascorbic Acid, Heparin). MSCs were cultured in alpha-MEM (Life Technologies), supplemented with 10% FCS, 100 U ml^{-1} penicillin, 100 µg ml^{-1} streptomycin, 0.2mM L-ascorbic acid-2-phosphate and 1 ng ml^{-1} basic fibroblast growth factor (bFGF, R&D Systems). ACPCs were obtained from the articular cartilage in the metacarpal joint of deceased equine donors as previously described [22], donated to science by their owner, in accordance to the ethical guidelines of the School of Veterinary Medicine of Utrecht University. ACPCs were expanded in Dulbecco Modified Eagle Media, supplemented with 10% FCS, 100 U ml^{-1} penicillin, 100 µg ml^{-1} streptomycin, 0.2 mM L-ascorbic acid-2-phosphate and 2.5 ng ml^{-1} bFGF. Cells were cultured up to passage 3 before bioprinting.

2.6. ECFC attachment study on DLP printed scaffold

ECFCs were seeded onto the hydrogel surfaces at a density of 150 cells mm^{-2}. After 1 and 3 days in culture, the samples were washed with PBS and a live/dead assay was conducted using 1ug ml^{-1} of calcein-AM and propidium iodide. Images were taken using a BX51 microscope (Olympus, Zoeterwoude, The Netherlands). The amount of cells attached on the sample surfaces were counted using ImageJ.

2.7. DLP bioprinting

Cylindrical samples (diameter = 5 mm, height = 1 mm) were produced to test cell viability upon encapsulation, while larger structures were fabricated to evaluate 3D cell distribution (5mm x 5mm x 5mm, 1.5h printing time). MSCs were mixed with the bio-resin at a final density of 5 x 10^6 cells/ml prior to light projection, then samples were placed in culture and at 1, 7 and 14 days, tested for live/dead staining (calcein-AM/ethidium homodimer). To assess cell distribution, constructs were fixed in formalin, stained with ethidium homodimer, and cross-sections of the large construct were

cut with a razor blade and imaged with a fluorescent microscope. Each gel slab was divided into seven zones (from top to bottom in the printing direction) and cells in each zone were counted, and the percentage of cells found in each zone was reported. To study cell differentiation and tissue matrix deposition, MSCs and ACPCs were encapsulated at a density of 5 x 10^6 and 20 x 10^6 cells/ml and printed. MSC-laden samples were cultured in osteogenic conditioning media (alpha-MEM, supplemented with 10% FCS, 100U ml^{-1} penicillin, 100µg ml^{-1} streptomycin, 0.2mM L-ascorbic acid-2-phosphate, 20 mM β-glycerol phosphate, 100nM dexamethasone). After 7 days of culture, ALP expression was visualised by incubation with the Dako Basic Fuchsin kit (Dako, Heverlee, Belgium) for 1 hour at room temperature according to the manufacturer's protocol. After 21 days, samples were fixed in formalin and thin sections (10µm) were cut with a cryostat, then stained with Alizarin Red S to visualize the deposition of calcified matrix. ACPC-laden constructs were instead cultured for 21 days in chondrogenic differentiation medium, consisting of DMEM, supplemented with 1% Insulin-Transferrin-Selenous acid premix (ITS-premix, Corning), 100U ml^{-1} penicillin, 100µg ml^{-1} streptomycin, 0.2 mM L-ascorbic acid-2-phosphate, 100 nM dexamethasone and 10ng ml^{-1} transforming growth factor β1 (TGF-β1). After 21 days of culture, formalin-fixed samples were sectioned with a cryostat, and stained with Alcian Blue to observe the deposition of sulphated glycosaminoglycans.

2.8. Statistical analysis

All data are represented as average and standard deviation of independent replicates (n=3 to 5). Statistical analysis was performed using the GraphPad Prism 6 software package, and performing a one-way analysis of variance (ANOVA). A significance level of 0.05 and a Tukey's post hoc analysis was used for all tests.

3. Result and discussion

3.1. Synthesis of PVA-MA and Gel-MA

PVA is investigated as a promising biomaterial for tissue engineering of multiple tissues including cartilage [23–25] and bone [26,27]. PVA has pendant hydroxyl groups that can be further chemically modified with a range of functional groups, such as vinyl sulfone [28], ester acrylate [29], and tyramine [30]. In this study, we chose to graft methacrylate groups onto PVA, where the resultant PVA-MA is well-established to be a cyto-compatible, water soluble macromer with low batch-to-batch variability, allowing simple hydrogel synthesis with tailorable physico-mechanical properties [31,32]. The synthesis of PVA-MA has been previously reported to be conducted in organic solvents, often due to the solubility of the methacrylate carries, such as 2-isocyanatoethyl methacrylate (ICEMA) [31] or glycidyl methacrylate (GMA) [33]. In this study, we successfully conjugated functional methacrylate groups onto PVA, using methacylic anhydride in a water based reaction, as observed by the peaks at $\delta = 6.1$ and 5.8 (Figure 2A & B). It was also observed that a minimum of 4 hours is required until the saturation point of the methacrylation reaction, where the degree of modification was quantified to be ~15% (Figure 2C). Previous study conducted by Nilasaroya *et al.* reported on synthesis of PVA-MA using GMA in water but required 7 days to obtain complete reaction [33].

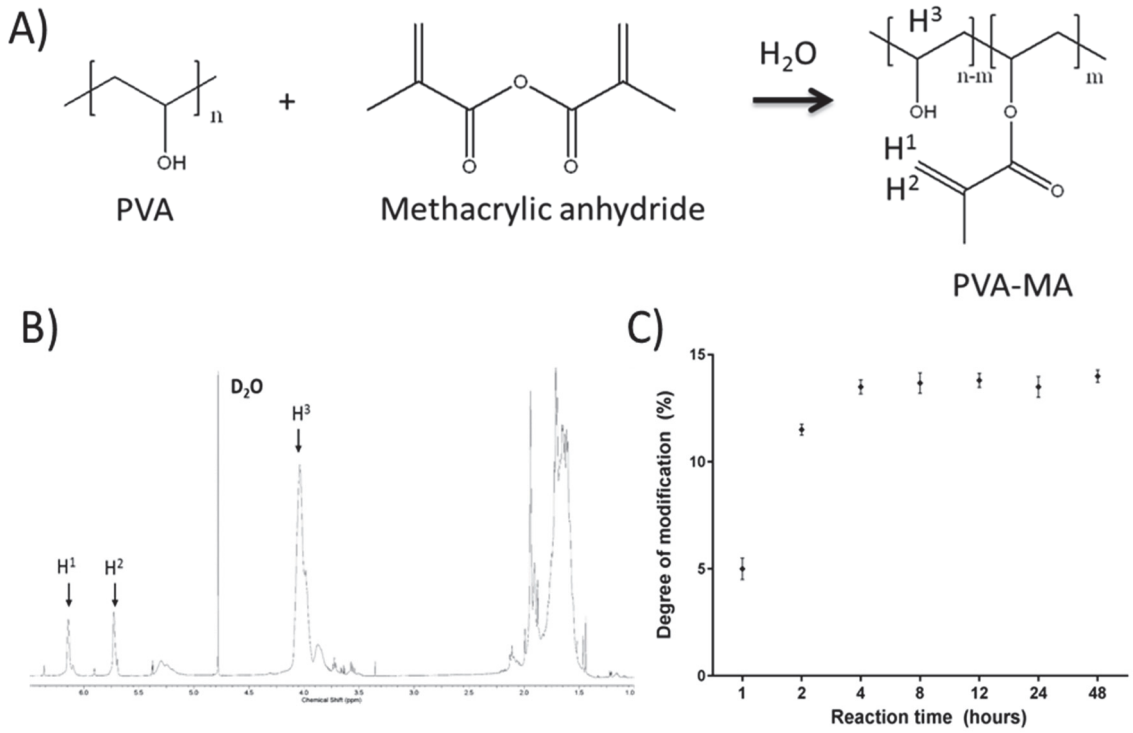

Figure 2: Schematic of PVA-MA synthesis route (A). ^{1}H-NMR spectra of PVA-MA (B), H^1 and H^2 represents protons of the methacrylate vinyl groups, indicating successful conjugation of methacrylate onto the PVA backbone. Degree of modification of PVA-MA over reaction time (C).

Similarly, Gel-MA was synthesised by reacting gelatin with methacrylic anhydride, a commonly used approach previously reported in the literature. Yue *et al.* has showed that methacrylic anhydride can react with primary amines, carboxyls and hydroxyls on gelatin, resulting in both functional methacrylate and methacrylamide groups. The GelMA component used in this study had a 60% degree of modification [34].

3.2. Fabrication of PVA-MA hydrogels using DLP lithography printing

A set of visible-light responsive photo-redox catalysts based on the transition metal complex (tris-bipyridyl-ruthenium (II) hexahydrate, Ru) combined with a persulfate compound (sodium persulfate, SPS) were selected as the photo-initiators. We have previously reported that these initiators absorb in 400 – 450nm of the visible light region [35,36], with exceptionally high molar extinction coefficient (ε = 14600$M^{-1}cm^{-1}$ at 450nm) compared to other conventionally used light responsive initiators [37–39].

Initially, a working curve for the PVA-MA bio-resin was evaluated to understand the curing properties. We hypothesise that only a low irradiation dosage is required to crosslink the bio-resin due to the high molar absorptivities of the Ru/SPS based photoinitiator utilized in this study. Figure 3 shows that the E_c for the bio-resin without the photo-absorber is 13mJ/cm^{-2}, which is significantly lower than previous values reported in the literature using the photoinitiator 1-[4-(2-hydroxyethoxy)-phenyl]-2-hydroxy-2-methyl-1-propane-1-one (I2959) and poly(ethylene glycol) based resin. Arcaute *et al.* reported that a minimum of 30.65mJ/cm^{-2} of UV light (365nm) was required to crosslink a resin consisting of 20wt% poly(ethylene glycol) dimethacrylate (PEG-DMA, Mw = 1000Da) and 0.5wt% I2959 [40]. Furthermore, Neiman *et al.* found that for 20wt% PEG-DMA of lower molecular weight (700Da) and 0.5wt% Irgacure 2959, at least 48mJ/cm^{-2} of UV light (325nm) was required to fabricate hydrogel constructs [39]. Both values are considerably higher than the critical energy required to crosslink the PVA-MA based bio-resin in this present study. However, we also observed that in order to improve the print resolution, a photo-absorber (1wt% Ponceau 4R) is required to be added to the bio-resin formulation (Figure 3). This addition resulted in an increment in the E_c to 110mJ/cm^2, which significantly reduced the light penetration depth (D_p), allowing better control over the printing resolution. As demonstrated in our attempt to print a simple cube computer-aided-design (CAD) model, the addition of photo-absorber is showed to be crucial to prevent unwanted over-curing of the bio-resin (Figure 3C&D). Similarly, Melchels *et al.* has previously reported that when printing polylactide-based resins, the addition of photo-absorber reduces the D_p and is required to produce constructs of high resolution [9].

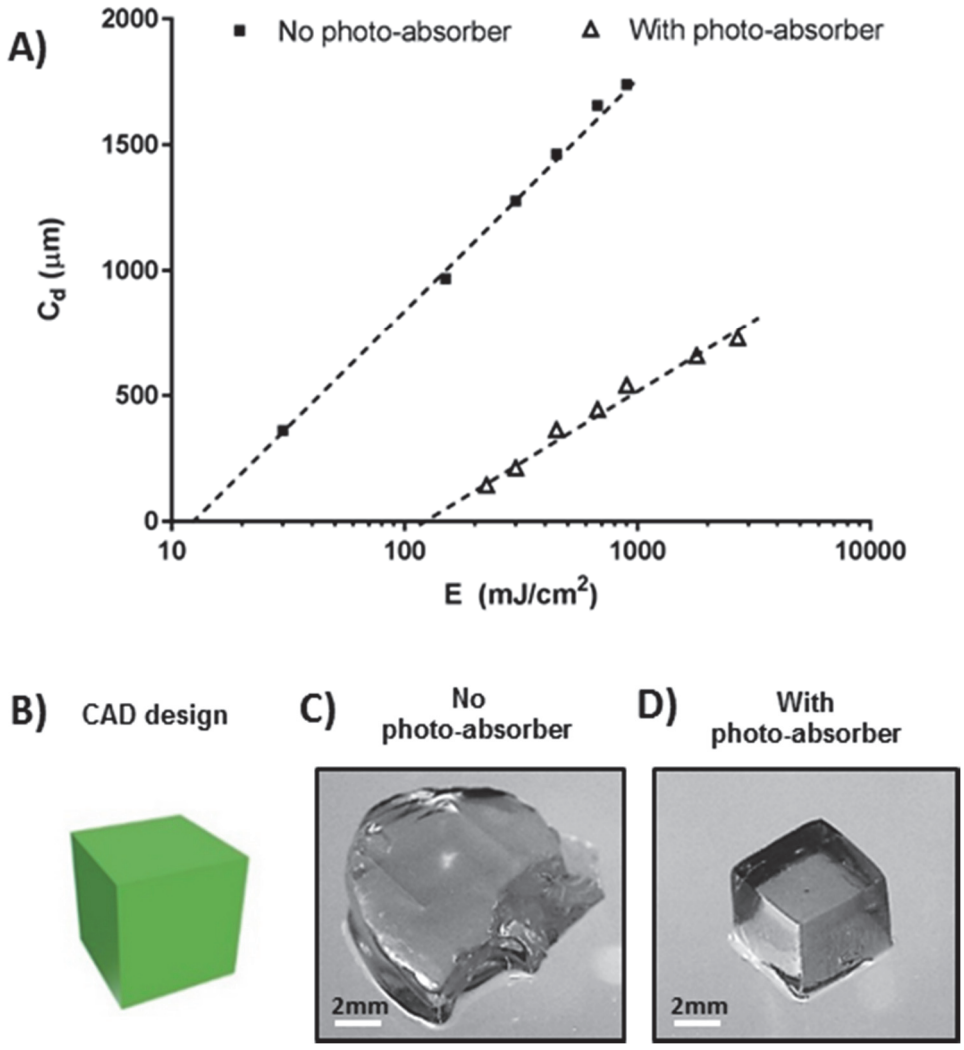

Figure 3: A) Working curve constructed for 10wt% PVA-MA + 0.2mM/2mM Ru/SPS with or without the photo-absorber (1wt% Ponceau 4R) using the Perfactory 3 Mini. B) CAD design of a cube. C) DLP printed cube construct without photo-absorber. D) DLP printed cube construct with photo-absorber.

We then investigated the possibility of DLP 3D printing of other solid hydrogel constructs such as the pyramid (Figure 4A-C) and cone (Figure 4D-F) using our formulated bio-resin. It was observed that constructs with distinct sharp edges can be fabricated, where the 50µm voxel step size was clearly visible in each constructs, demonstrating the precision that could be achieved. In figures 4H&I, we confirmed the possibility to fabricate hydrogels with channels (range = 50µm to 500µm) in a single print (Figure 4D1-D3, flower-like print, with alternated petals and channels). We also demonstrated that the open channels are capable to be infused with a secondary bioink (Figure S1).

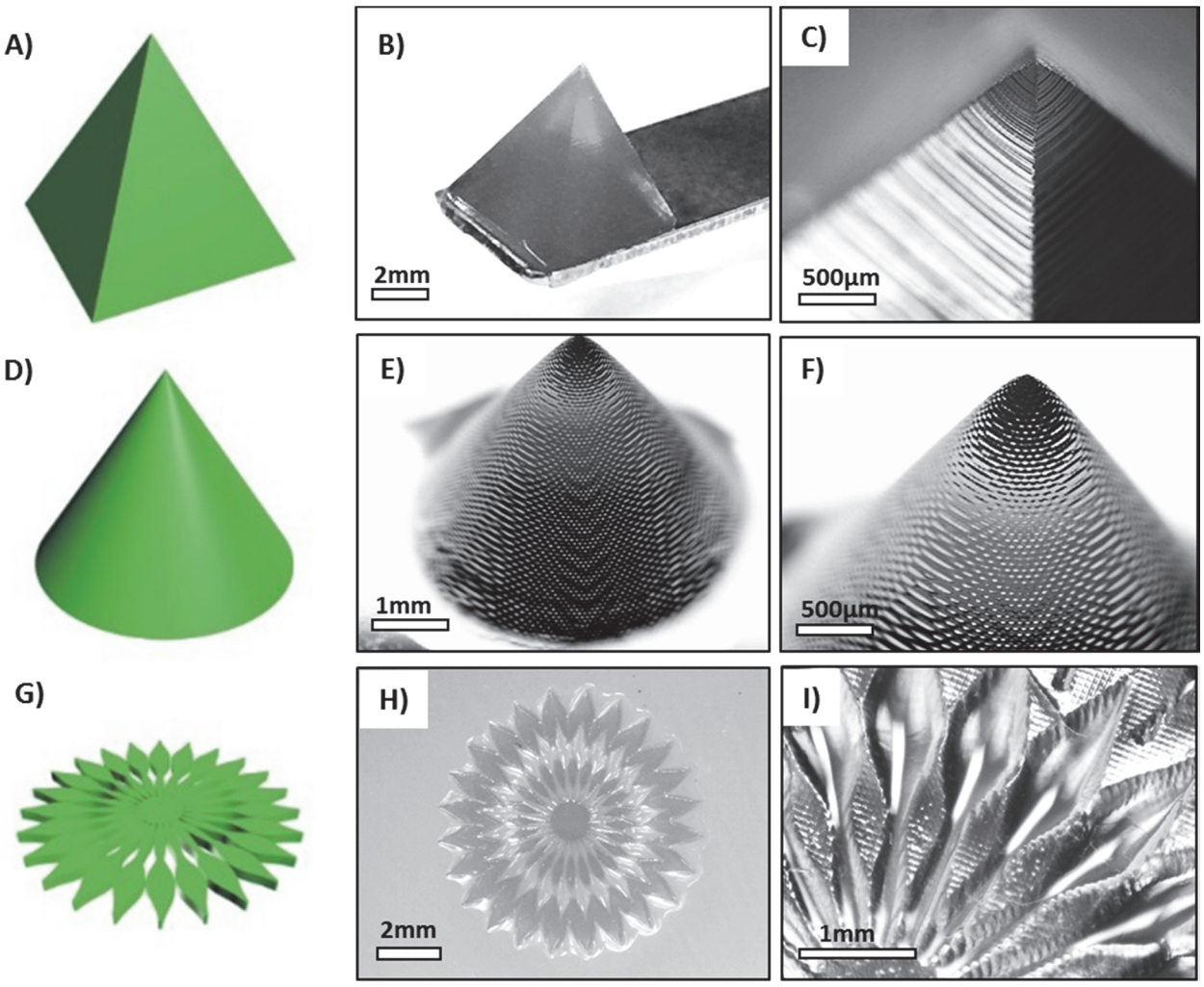

Figure 4: Fabrication of high resolution solid hydrogel structures: pyramid (A-C), cone (D-F), flower with channels having sizes ranging from 50 to 500µm (G-I).

3.3. Complex prints with high resolution

Moreover, further examples demonstrating the capability and sophistication of DLP printed hydrogel designs include the woven mat (Figure 5A-C) and ring mail (Figure 5D-F). These DLP-fabricated constructs are composed by intertwined struts, which cannot be obtained using nozzle-based additive manufacturing techniques, such as fused deposition modelling, inkjet or extrusion-based bioprinting. In particular, steps of 30µm were visible on the struts of the woven mat sample (Figure 5C), further outlining the high resolution that could be achieved using this technology. More importantly, the irradiation dosage used in this study was also sufficient to fabricate complex porous constructs via DLP as demonstrated by the tetragonal lattice in Figure 5G-I. In this scaffold, the strut diameter was 100µm and the distance between struts was 500µm. The observed porosity and

interconnected pore network are essential for supporting nutrient diffusion through the scaffold and convection within fabricated hydrogel struts [41].

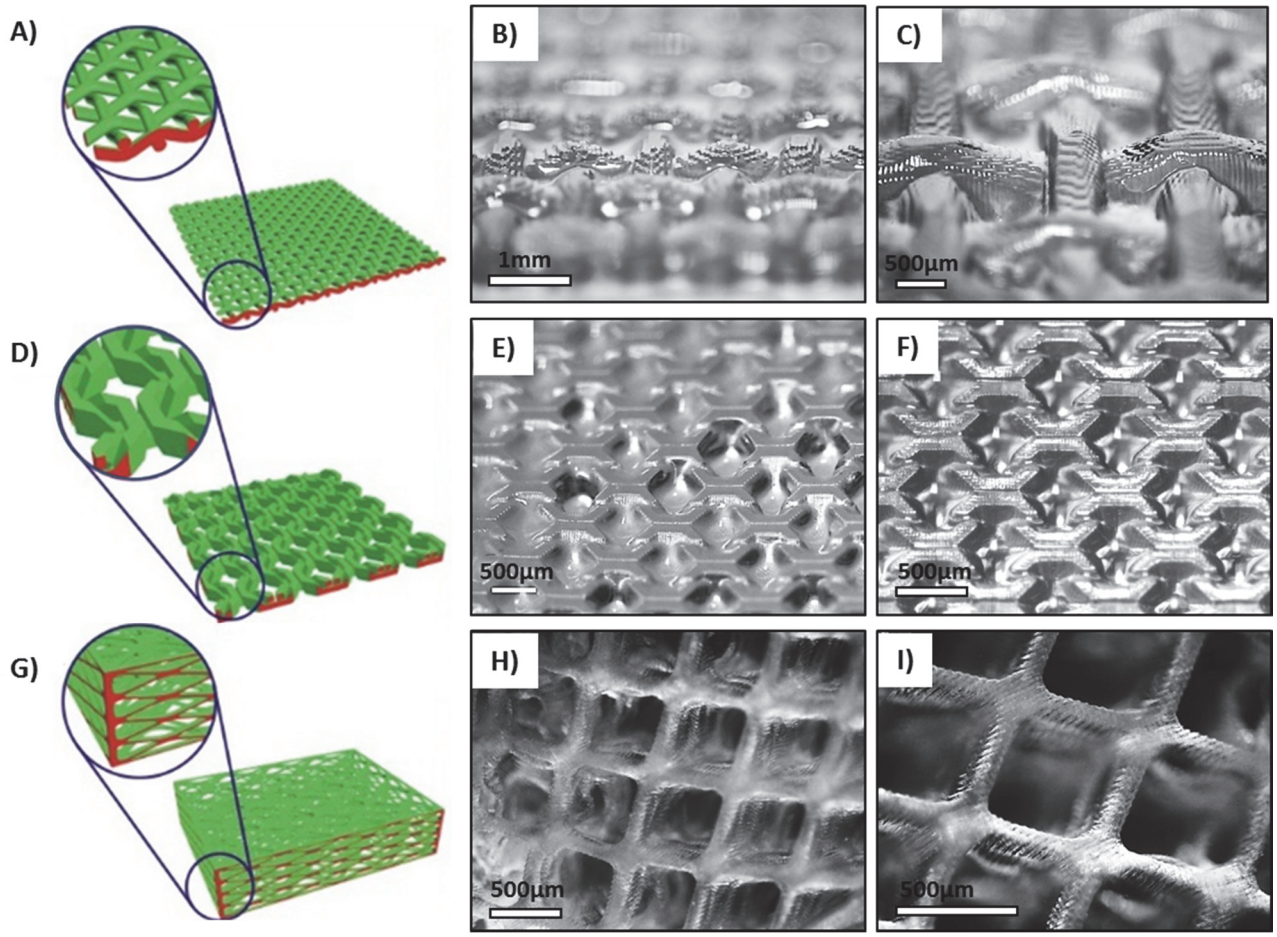

Figure 5: DLP-printing allowed to generate hydrogels with 3D patterns that are not achievable with extrusion-based printing systems, including woven mats (A-C), ring mails (D-F), and 3D lattice structures with arches oriented in the z-direction (G-I).

The resolution capability of the DLP bio-resins was further highlighted in porous gyroid scaffolds (Figure 6A-F), featuring highly curved surfaces, ordered pore size (500µm, Figure C&F) and high porosity. SEM images further confirmed the high resolution achieved where voxel sizes of 25µm were highly visible in the petals of the DLP 3D printed hydrogel gyroid (Figure 6D&E). The ability to fabricate gyroidal constructs at high resolution are of particular relevance given that previous studies have demonstrated that the unique gyroidal surface characteristics yield optimal nutrient flow profiles under perfusion, that are of interest for cell seeding and tissue engineering [9].

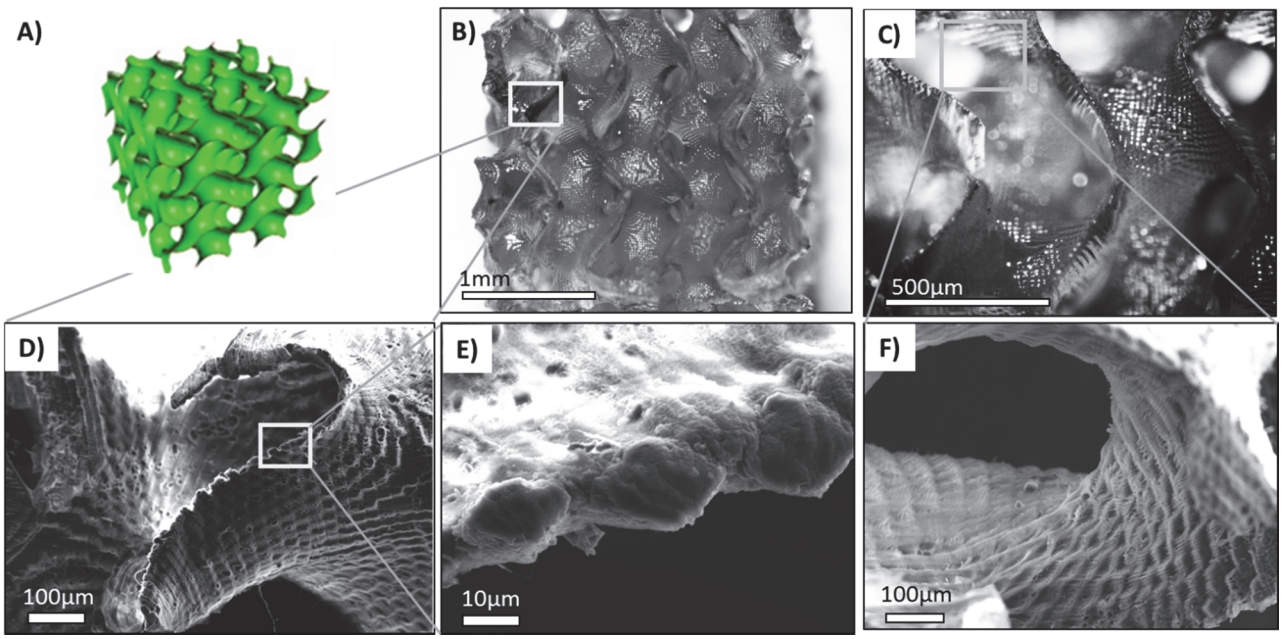

Figure 6: A) Gyroid construct, showing its complex porous pattern as imaged via B,C) optical microscopy, and D,E,F) Scanning Electron Miscroscopy. High-magnification SEM micrograph highlighted the surface morphology of the DLP-printed voxels that compose the 3D construct.

Lithography-based fabrication technology has been traditionally used for jewelry making and in the automotive industry with a range of commercially available resins [42,43]. However, these resins are often composed of organic solvents or toxic chemicals that are not suitable for biofabrication, where living cells are mixed within the bio-resin. For example, common DLP photo-initiators used, such as bis-acylphosphine oxide (BAPO) and ethyl-2,4,6-trimethylbenzoylphenylphosphinate (Lucirin TPO-L) require toxic organic solvents such as dichloromethane or acetonitrile for dissolution [10,44]. In order to fabricate cell-laden hydrogel constructs, the bio-resin ideally should be water soluble, which greatly reduces the number of suitable photo-initiators. To date, the two most popular water soluble photo-initiators used for DLP printing are I2959 and lithium phenyl-2,4,6-trimethylbenzoyl-phosphinate (LAP). However, the molar absorptivity of both I2959 ($\varepsilon = 4 M^{-1}cm^{-1}$ at 365nm) and LAP ($\varepsilon = 50 M^{-1}cm^{-1}$ at 405nm) is relatively weak, leading to poor reactivity [37]. As a result, higher initiator concentration, irradiation intensity and longer irradiation times are required to achieve a high degree of crosslinking. This poor photo-reactivity also limits achievable resolutions to 150-300µm and is detrimental to the generation of large, thick constructs of high shape fidelity required for clinical translation of biofabrication [11,40].

In this study, the set of Ru/SPS photo-initiators employed has significantly higher molar absorptivity, approximately 300-fold higher than LAP. Additionally, the DLP technology allows fabrication of multiple constructs on one base platform, which can be used to fabricate multiple cellular modules for high throughput testing of tissue models or 3D bioassembly [45].

3.3. Biofunctionalisation of DLP 3D printed PVA constructs with Gel-MA

PVA-MA is a synthetic polymer lacking biological recognition sites for cellular signaling and function [46]. Thus, gelatin-methacryloyl (Gel-MA), which has been previously reported to support cell adhesion, growth and proliferation [47], was co-polymerized with PVA-MA to impart bio-functionality into the resultant biosynthetic hydrogels. However, one concern was whether the incorporation of 1wt% Gel-MA into the PVA-MA based bio-resin would perturb the overall crosslinking reaction, and detrimentally affect print fidelity of DLP printed PVA-MA hydrogels shown earlier. Hence, sol-gel analysis was conducted to evaluate the physico-mechanical properties of both PVA-MA and PVA-MA/Gel-MA hydrogel discs fabricated using DLP. There are no significant differences with respect to viscosity of the bio-resin (Figure 7A), sol fraction (~25%, Figure 7B), mass swelling ratio (~9, Figure 7C), mesh size (~260Å, Figure 7D) and crosslinking density (~1.3 mol L^{-1}, Figure 7E) between samples with or without Gel-MA. This could be expected as Gel-MA has methacryloyl groups (methacrylates and methacrylamides) chemically grafted to its polymer backbone [34], which can take part in the formation of covalent crosslinks with PVA-MA during the photo-initiated radical polymerization reaction. As the concentration of Gel-MA added into the PVA-MA based bio-resin is only 1wt%, it was anticipated that such small quantity will not affect the crosslinking mechanics and overall physico-chemical property of the printed construct. However, this minor increment in the total polymer concentration was correlated with a significant increment in the mechanical stiffness, when compared to that of pure PVA-MA gels (Figure 7F).

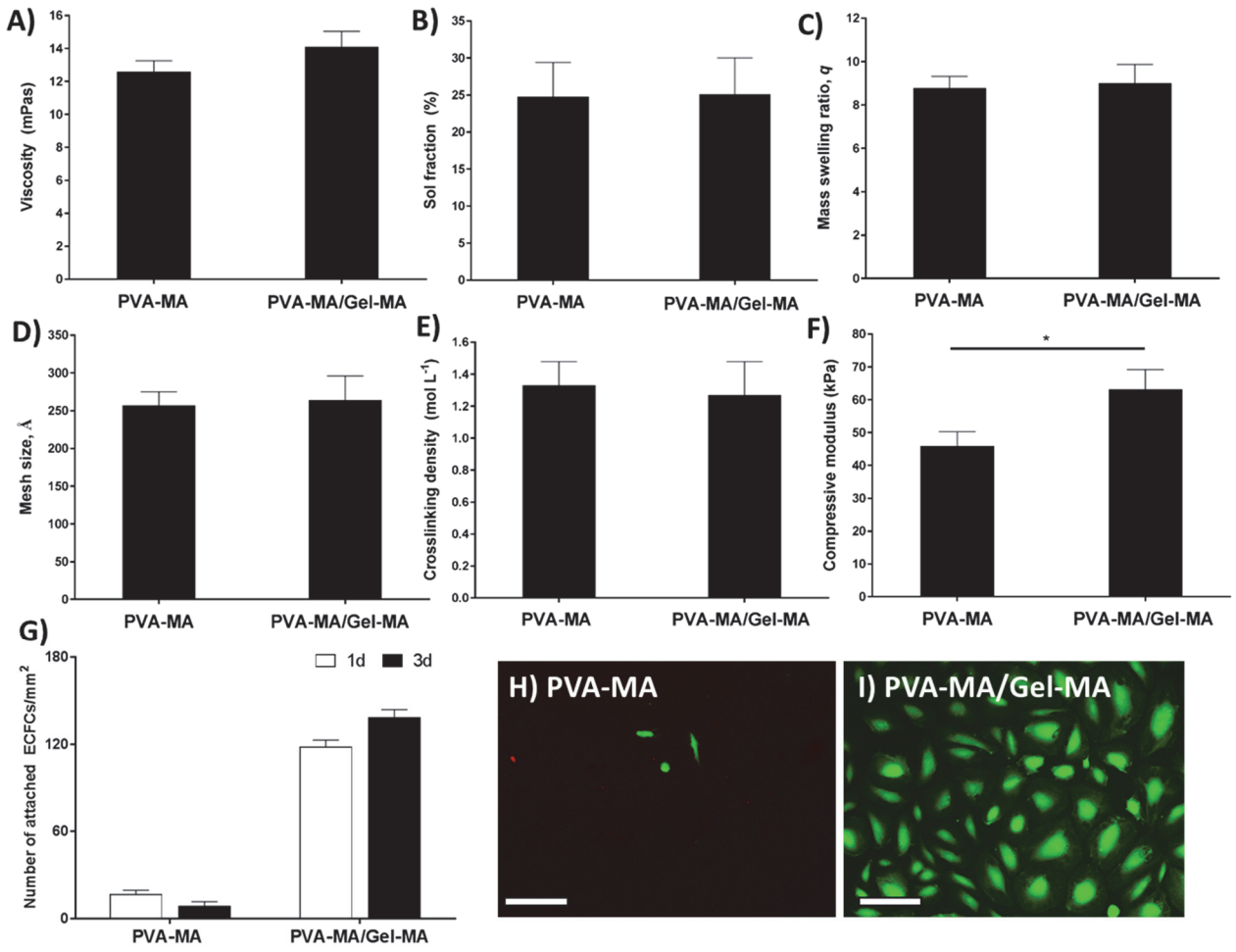

Figure 7: Physico-chemical and mechanical properties of DLP 3D printed PVA-MA or PVA-MA/Gel-MA constructs (A-F). ECFC attachment (G) and live/dead images of ECFC on DLP printed PVA-MA (H) or PVA-MA/Gel-MA (I) hydrogel constructs after 3days. Live = green; Dead = red.

Next, we evaluated the biofunctionality of the DLP 3D printed scaffolds with an initial 2D cell adhesion study, where endothelial colony forming cells (ECFCs) were seeded onto DLP printed PVA-MA or PVA-MA/Gel-MA discs. After 1 day of culture, less than 10% of seeded cells were attached onto pure PVA-MA gels, as expected, due to its highly hydrophilic nature and lack of bioactive sites (Figure 7G&H) [48,49]. However, addition of 1wt% Gel-MA into the PVA-MA gels increased the percentage of adhered cells to 80% (Figure 7G&I). This result indicated that the incorporated Gel-MA remained bioactive after the DLP process, and cell adhesive peptide sequences (e.g. Arginine-Glycine-Aspartic acid, RGD) were not only present in the bulk of the printed gels, but also accessible to the cells on the surface. This observation also further confirms that the Gel-MA was indeed covalently co-polymerised within the PVA-MA hydrogel network.

The resolution of the DLP printing process was also shown to not be affected by the presence of Gel-MA. PVA-MA/Gel-MA hydrogel structures with a resolution of 25 - 50μm was successfully DLP 3D printed using the identical printing parameters (i.e. exposure time and light intensity) for the formulated bio-resin without Gel-MA (Figure S2).

3.4. DLP 3D bioprinting of cell-laden hydrogel constructs

Cell culture studies demonstrated the capability for bioprinting of cell-laden constructs via DLP, using our novel bio-resin/photoinitiator pair. Human bone marrow derived mesenchymal stromal cells (MSCs) were firstly encapsulated into the PVA-MA based hydrogel constructs via DLP bioprinting. We observed that the PVA-MA based bio-resins were non cytotoxic to MSCs irrespective of whether 1wt% Gel-MA was added, with > 85% cell viability observed in biofabricated constructs 1 day post printing. However, it is important to note that the addition of 1wt% Gel-MA was crucial to support long term survival of encapsulated cells. For example, in pure PVA-MA gels, MSC viability decreased from 87 ± 3% (day 1) to 71 ± 7% (day 14), whereas the viability of cells encapsulated within PVA-MA/Gel-MA samples remained at 92 ± 3% after 14 days in culture (Figure 8A-C). Nevertheless, both samples were able to support osteogenic differentiation of the encapsulated MSCs as reflected in positive staining of alkaline phosphatase (Figure 8D&E) and alizarin red (Figure 8F&G). In order to test the potential of the bio-resin to support cartilage tissue formation, articular cartilage-derived chondroprogenitor cells (ACPCs) [22], were also encapsulated within PVA-MA/Gel-MA. Encapsulated ACPCs were able to produce extracellular matrix indicated by the positive staining of sulfated glycosaminoglycan (Figure 8H&I). These results highlight the potential of DLP bio-resins described herein for biofabrication of cell-laden hydrogel constructs for both bone and cartilage engineering.

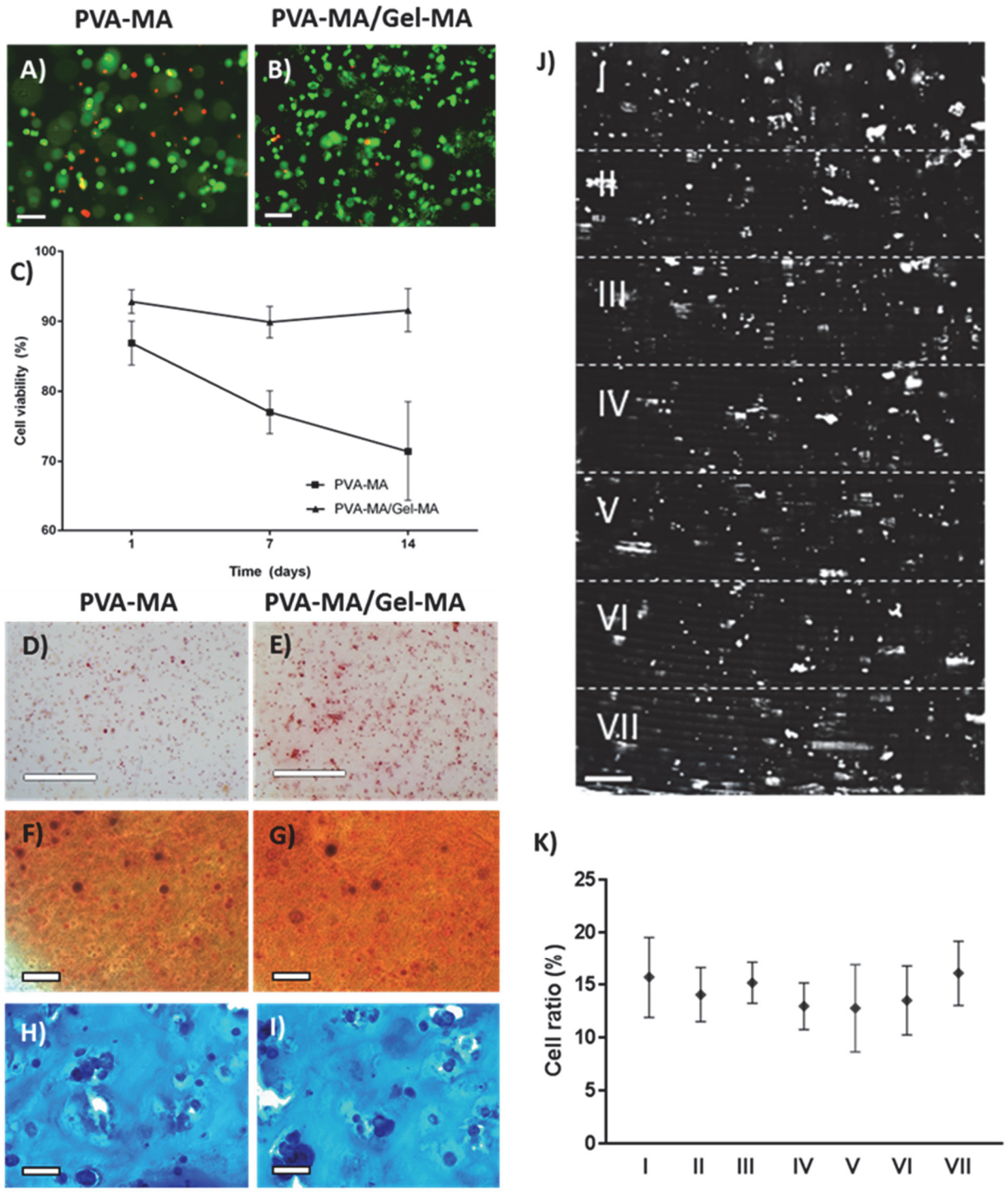

Figure 8. Cell encapsulation in printed hydrogel constructs. Live/dead images of printed MSCs cultured in osteogenic differentiation media after 14 days, Scale bar = 100µm: PVA-MA (A), PVA-MA/Gel-MA (B). Viability of MSCs over a culture period of 14 days (C). Alkaline phosphatase staining (red) of MSCs encapsulated in PVA-MA (D) and PVA-MA/Gel-MA (E) after 7 days, scale bar = 500µm. Alizarin red staining (red) of MSCs encapsulated in PVA-MA (F) and PVA-MA/Gel-MA (G) after 7 days, scale bar = 100 µm. Alcian blue staining (blue) of ACPCs encapsulated in PVA-MA (H) and PVA-MA/Gel-MA (I) after 21 days of culture in chondrogenic differentiation media, scale bar = 100µm. Cross-section image of construct, showing the whole height of the 5 mm x 5 mm x 5mm cell-laden cube (J). Cells were fixed, and stained with ethidium homodimer and the section was divided into 7 different zones (700µm height each). Percentage of cells present in each zone, relative to the total cell amount in the whole cross-section (K), scale bar = 200µm.

Bio-resins should preferably display Newtonian fluid characteristics with sufficiently low viscosity to flow under gravity between successive polymerization steps, to allow a fresh resin level to be established and also to drain non-polymerized resin from the biofabricated part. In this study, although we demonstrated that PVA-MA bio-resin flow properties supported native 30μm step size resolutions similar to commercial resins for standard DLP, there was a potential risk of cell settling or sedimentation during DLP biofabrication, particularly when printing thick constructs needed for tissue engineering. For example, Chan *et al.* previously reported that in a typical top-down stereolithography approach, cells mixed within the resin settle to the bottom of the resin reservoir during the printing process, causing inhomogeneous cell distribution within the printed construct [50]. In addition, Lin *et al.* showed that 37.5% (v/v) of Percoll was required as an additive in a PEG based resin to match the buoyant density of the cells to prevent cell settling [11]. Therefore, the distribution of cells within the DLP hydrogel constructs was examined. We demonstrated that without addition of any buoyancy-modifying component to the bio-resin, cells remained homogenously distributed throughout biofabricated hydrogel constructs. Figure 8J shows the cross-section of a 5mm thick hydrogel construct where the percentage of cells present in each zone (I – VII) from top to bottom remained constant despite the long printing time (1.5h to obtain a thick 5mm x 5mm x 5mm cube). This data indicates that the viscosity of the developed bio-resin, combined with the gentle movement of the DLP platform, were sufficient to maintain a homogenous cell suspension.

4. Conclusions

This study describes the development and characterization of a bio-resin based on PVA-MA, Gel-MA and Ru/SPS with demonstrated compatibility with commercial DLP technology. DLP of bio-resins allowed biofabrication of constructs with higher resolution and shape fidelity (down to 25μm) compared to existing extrusion-based 3D bioprinting technologies. Furthermore, DLP of cell-laden bio-resin hydrogels supported long-term cell survival, promoted chondrogenic and osteogenic differentiation, indicating potential applications in osteochondral tissue engineering, as well as the capability to biofabricate thick constructs with homogeneous cell distribution.

Acknowledgements

KSL and RL contributed equally to the idea, experimental design and execution of this study. The manuscript was written through contributions of all authors. All authors have given approval to the final version of the manuscript. This work was financially supported by the New Zealand Health Research Council Emerging Researcher First Grant (KL15/083; KL), the Royal Society of New Zealand Rutherford Discovery Fellowship (RDF-UOO1204; TW), as well as the European Union's Seventh Framework Programme FP7-MC-IRSES under grant agreement n°318553 (project skelGEN).

References

[1] Groll J, Boland T, Blunk T, Burdick J A, Cho D-W, Dalton P D, Derby B, Forgacs G, Li Q, Mironov V A, Moroni L, Nakamura M, Shu W, Takeuchi S, Vozzi G, Woodfield T B F, Xu T, Yoo J J and Malda J 2016 Biofabrication: reappraising the definition of an evolving field *Biofabrication* **8** 13001

[2] Costa P F, Vaquette C, Baldwin J, Chhaya M, Gomes M E, Reis R L, Theodoropoulos C and Hutmacher D W 2014 Biofabrication of customized bone grafts by combination of additive manufacturing and bioreactor knowhow *Biofabrication* **6** 35006

[3] Schuurman W, Levett P A, Pot M W, van Weeren P R, Dhert W J A, Hutmacher D W, Melchels F P W, Klein T J and Malda J 2013 Gelatin-Methacrylamide Hydrogels as Potential Biomaterials for Fabrication of Tissue-Engineered Cartilage Constructs *Macromol. Biosci.* **13** 551–61

[4] Bertassoni L E, Cecconi M, Manoharan V, Nikkhah M, Hjortnaes J, Cristino A L, Barabaschi G, Demarchi D, Dokmeci M R, Yang Y and Khademhosseini A 2014 Hydrogel bioprinted microchannel networks for vascularization of tissue engineering constructs. *Lab Chip* **14** 2202–11

[5] Billiet T, Gevaert E, De Schryver T, Cornelissen M and Dubruel P 2014 The 3D printing of gelatin methacrylamide cell-laden tissue-engineered constructs with high cell viability *Biomaterials* **35** 49–62

[6] Lim K S, Schon B S, Mekhileri N V, Brown G C J, Chia C M, Prabakar S, Hooper G J and Woodfield T B F 2016 New Visible-Light Photoinitiating System for Improved Print Fidelity in Gelatin-Based Bioinks *ACS Biomater. Sci. Eng.* **2** 1752–62

[7] Mouser V H M, Melchels F P W, Visser J, Dhert W J A, Gawlitta D and Malda J 2016 Yield stress determines bioprintability of hydrogels based on gelatin-methacryloyl and gellan gum for cartilage bioprinting *Biofabrication* **8** 35003

[8] Mouser V H M, Abbadessa A, Levato R, Hennink W E, Vermonden T, Gawlitta D and Malda J 2017 Development of a thermosensitive HAMA-containing bio-ink for the fabrication of composite cartilage repair constructs *Biofabrication* **9** 15026

[9] Melchels F P W, Feijen J and Grijpma D W 2009 A poly(d,l-lactide) resin for the preparation of tissue engineering scaffolds by stereolithography *Biomaterials* **30** 3801–9

[10] Melchels F P W, Feijen J and Grijpma D W 2010 A review on stereolithography and its applications in biomedical engineering *Biomaterials* **31** 6121–30

[11] Lin H, Zhang D, Alexander P G, Yang G, Tan J, Cheng A W-M and Tuan R S 2013 Application of visible light-based projection stereolithography for live cell-scaffold fabrication with designed architecture *Biomaterials* **34** 331–9

[12] Zorlutuna P, Jeong J H, Kong H and Bashir R 2011 Stereolithography-Based Hydrogel Microenvironments to Examine Cellular Interactions *Adv. Funct. Mater.* **21** 3642–51

[13] Malda J, Visser J, Melchels F P, Jüngst T, Hennink W E, Dhert W J A, Groll J and Hutmacher D W 2013 25th Anniversary Article: Engineering Hydrogels for Biofabrication *Adv. Mater.* **25** 5011–28

[14] Ouyang L, Highley C B, Rodell C B, Sun W and Burdick J A 2016 3D Printing of Shear-Thinning Hyaluronic Acid Hydrogels with Secondary Cross-Linking *ACS Biomater. Sci. Eng.* **2** 1743–51

[15] Bertlein S, Brown G, Lim K S, Jungst T, Boeck T, Blunk T, Tessmar J, Hooper G J, Woodfield T B F and Groll J 2017 Thiol–Ene Clickable Gelatin: A Platform Bioink for Multiple 3D Biofabrication Technologies *Adv. Mater.* **29**

[16] Pawar A A, Saada G, Cooperstein I, Larush L, Jackman J A, Tabaei S R, Cho N-J and Magdassi S 2016 High-performance 3D printing of hydrogels by water-dispersible photoinitiator nanoparticles *Sci. Adv.* **2** e1501381–e1501381

[17] Billiet T, Vandenhaute M, Schelfhout J, Van Vlierberghe S and Dubruel P 2012 A review of trends and limitations in hydrogel-rapid prototyping for tissue engineering *Biomaterials* **33**

6020–41
[18] Lim K S, Roberts J J, Alves M-H, Poole-Warren L A and Martens P J 2015 Understanding and tailoring the degradation of PVA-tyramine hydrogels *J. Appl. Polym. Sci.* **132**n/a-n/a
[19] Peppas N A and Merrill E W 1976 Poly(vinyl alcohol) hydrogels: Reinforcement of radiation-crosslinked networks by crystallization *J. Polym. Sci. Polym. Chem. Ed.* **14** 441–57
[20] de Jonge N, Muylaert D E P, Fioretta E S, Baaijens F P T, Fledderus J O, Verhaar M C and Bouten C V C 2013 Matrix Production and Organization by Endothelial Colony Forming Cells in Mechanically Strained Engineered Tissue Constructs ed S Kumar *PLoS One* **8** e73161
[21] Gawlitta D, Benders K E M, Visser J, van der Sar A S, Kempen D H R, Theyse L F H, Malda J and Dhert W J A 2015 Decellularized cartilage-derived matrix as substrate for endochondral bone regeneration. *Tissue Eng. Part A* **21** 694–703
[22] Levato R, Webb W R, Otto I A, Mensinga A, Zhang Y, van Rijen M, van Weeren R, Khan I M and Malda J 2017 The bio in the ink: cartilage regeneration with bioprintable hydrogels and articular cartilage-derived progenitor cells *Acta Biomater.* **61** 41–53
[23] Huang X, Hou Y, Zhong L, Huang D, Qian H, Karperien M and Chen W 2018 Promoted Chondrogenesis of Cocultured Chondrocytes and Mesenchymal Stem Cells under Hypoxia Using In-situ Forming Degradable Hydrogel Scaffolds *Biomacromolecules* **19** 94–102
[24] Lee J, Sultan M, Kim S, Kumar V, Yeon Y, Lee O and Park C 2017 Artificial Auricular Cartilage Using Silk Fibroin and Polyvinyl Alcohol Hydrogel *Int. J. Mol. Sci.* **18** 1707
[25] Yuan F, Ma M, Lu L, Pan Z, Zhou W, Cai J, Luo S, Zeng W and Yin F 2017 Preparation and properties of polyvinyl alcohol (PVA) and hydroxylapatite (HA) hydrogels for cartilage tissue engineering. *Cell. Mol. Biol. (Noisy-le-grand).* **63** 32–5
[26] Bendtsen S T, Quinnell S P and Wei M 2017 Development of a novel alginate-polyvinyl alcohol-hydroxyapatite hydrogel for 3D bioprinting bone tissue engineered scaffolds *J. Biomed. Mater. Res. Part A* **105** 1457–68
[27] Oh S H, An D B, Kim T H and Lee J H 2016 Wide-range stiffness gradient PVA/HA hydrogel to investigate stem cell differentiation behavior *Acta Biomater.* **35** 23–31
[28] Imai K, Shiomi T, Tezuka Y and Takada M 1988 Synthesis of sulfone-modified poly(vinyl alcohol) and its application for permselective membrane of sulfur dioxide *J. Appl. Polym. Sci.* **35** 1817–28
[29] Martens P, Holland T and Anseth K S 2002 Synthesis and characterization of degradable hydrogels formed from acrylate modified poly(vinyl alcohol) macromers *Polymer (Guildf).* **43** 6093–100
[30] Lim K S, Roberts J J, Alves M-H, Poole-Warren L A and Martens P J 2015 Understanding and tailoring the degradation of PVA-tyramine hydrogels *J. Appl. Polym. Sci.* **132**n/a-n/a
[31] Lim K S, Kundu J, Reeves A, Poole-Warren L A, Kundu S C and Martens P J 2012 The influence of silkworm species on cellular interactions with novel PVA/silk sericin hydrogels. *Macromol. Biosci.* **12** 322–32
[32] Chong S-F, Smith A A A and Zelikin A N 2013 Microstructured, Functional PVA Hydrogels through Bioconjugation with Oligopeptides under Physiological Conditions *Small* **9** 942–50
[33] Nilasaroya A, Poole-Warren L A, Whitelock J M and Jo Martens P 2008 Structural and functional characterisation of poly(vinyl alcohol) and heparin hydrogels *Biomaterials* **29** 4658–64
[34] Yue K, Li X, Schrobback K, Sheikhi A, Annabi N, Leijten J, Zhang W, Zhang Y S, Hutmacher D W, Klein T J and Khademhosseini A 2017 Structural analysis of photocrosslinkable methacryloyl-modified protein derivatives *Biomaterials* **139** 163–71
[35] Lim K S, Ramaswamy Y, Roberts J J, Alves M-H, Poole-Warren L A and Martens P J 2015 Promoting Cell Survival and Proliferation in Degradable Poly(vinyl alcohol)-Tyramine Hydrogels *Macromol. Biosci.* **15** 1423–32
[36] Lim K S, Levato R, Costa P F, Castilho M, Dorenmalen K, Melchels F P W, Gawlitta D,

Malda J and Woodfield T B F 2016 Biofabrication of Hydrogel Based "Bio-resins" via High Resoution Digital Light Processing *Frontiers in Bioengineering and Biotechnology*

[37] Fairbanks B D, Schwartz M P, Bowman C N and Anseth K S 2009 Photoinitiated polymerization of PEG-diacrylate with lithium phenyl-2,4,6-trimethylbenzoylphosphinate: polymerization rate and cytocompatibility *Biomaterials* **30** 6702–7

[38] Müller P and Brettel K 2012 [Ru(bpy)3]2+ as a reference in transient absorption spectroscopy: differential absorption coefficients for formation of the long-lived 3MLCT excited state *Photochem. Photobiol. Sci.* **11** 632

[39] Neiman J A S, Raman R, Chan V, Rhoads M G, Raredon M S B, Velazquez J J, Dyer R L, Bashir R, Hammond P T and Griffith L G 2015 Photopatterning of hydrogel scaffolds coupled to filter materials using stereolithography for perfused 3D culture of hepatocytes *Biotechnol. Bioeng.* **112** 777–87

[40] Arcaute K, Mann B K and Wicker R B 2006 Stereolithography of Three-Dimensional Bioactive Poly(Ethylene Glycol) Constructs with Encapsulated Cells *Ann. Biomed. Eng.* **34** 1429–41

[41] Loh Q L and Choong C 2013 Three-dimensional scaffolds for tissue engineering applications: role of porosity and pore size. *Tissue Eng. Part B. Rev.* **19** 485–502

[42] Gauvin R, Chen Y-C, Lee J W, Soman P, Zorlutuna P, Nichol J W, Bae H, Chen S and Khademhosseini A 2012 Microfabrication of complex porous tissue engineering scaffolds using 3D projection stereolithography *Biomaterials* **33** 3824–34

[43] Sun A X, Lin H, Beck A M, Kilroy E J and Tuan R S 2015 Projection Stereolithographic Fabrication of Human Adipose Stem Cell-Incorporated Biodegradable Scaffolds for Cartilage Tissue Engineering *Front. Bioeng. Biotechnol.* **3** 115

[44] Cooke M N, Fisher J P, Dean D, Rimnac C and Mikos A G 2003 Use of stereolithography to manufacture critical-sized 3D biodegradable scaffolds for bone ingrowth *J. Biomed. Mater. Res.* **64B** 65–9

[45] Mekhileri N V, Lim K S, Brown G C J, Mutreja I, Schon B S, Hooper G J and Woodfield T B F 2018 Automated 3D bioassembly of micro-tissues for biofabrication of hybrid tissue engineered constructs *Biofabrication* **10** 24103

[46] Lim K S, Alves M H, Poole-Warren L A and Martens P J 2013 Covalent incorporation of non-chemically modified gelatin into degradable PVA-tyramine hydrogels *Biomaterials* **34** 7097–105

[47] Nichol J W, Koshy S T, Bae H, Hwang C M, Yamanlar S and Khademhosseini A 2010 Cell-laden microengineered gelatin methacrylate hydrogels *Biomaterials* **31** 5536–44

[48] Hayami T, Matsumura K, Kusunoki M, Nishikawa H and Hontsu S 2007 Imparting cell adhesion to poly(vinyl alcohol) hydrogel by coating with hydroxyapatite thin film *Mater. Lett.* **61** 2667–70

[49] Nuttelman C R, Henry S M and Anseth K S 2002 Synthesis and characterization of photocrosslinkable, degradable poly(vinyl alcohol)-based tissue engineering scaffolds *Biomaterials* **23** 3617–26

[50] Chan V, Zorlutuna P, Jeong J H, Kong H and Bashir R 2010 Three-dimensional photopatterning of hydrogels using stereolithography for long-term cell encapsulation *Lab Chip* **10** 2062